GEOPHYSICS, VOL. 52, NO. 12 (DECEMBER 1987); P. 1689–1696, 5 FIGS., 2 TABLES.

The radiation characteristics of an arbitrary antenna positioned on a polar ice sheet

James C. West* and Kenneth R. Demarest*

ABSTRACT

The radiation pattern of an arbitrarily shaped antenna system placed directly on the surface of a polar ice sheet (a configuration often used for ice-probing radars) may be determined at any depth within the ice sheet using a two-step process. The distribution of the radiated field just beneath the surface may be determined first using the method of moments, and geometric optics can then be used to calculate the effects of the exponential density gradient of the ice. Closed-form solutions of the ray-tracing equation, valid at any depth within the ice sheet, allow rapid calculation of the effective look angles and gain increases of any antenna mounted on the surface. These solutions asymptotically approach previously determined relations which are valid only at great depths. A numerical example demonstrates the use of this procedure in the design of a practical ice-probing radar antenna system.

INTRODUCTION

Radar techniques have been used to investigate the structures of the polar ice sheets since the 1950s. Although initially used to determine the thickness of the ice sheet (Evans, 1963), radar has also been used to examine internal layers within the ice (Harrison, 1973) and to locate crevasses beneath the surface. Bogorodsky et al. (1985) have summarized the various systems used for ice probing in the past.

To maximize the penetration range, probing radars often use antennas located directly on the ice surface, thus eliminating any spreading losses for propagation within the air and reflection losses from the surface itself (Robin et al., 1969). However, since the permittivity of the ice is greater than that of free space, the radiation into the ice surface is greater than would be expected from the free-space radiation pattern of the antenna. Furthermore, the permittivity of the ice is not constant but changes with depth. Hence, the energy is refracted as it propagates downward, further modifying the characteristics of the radiation.

Since many aspects of the performance of a probing radar are determined by the radiation pattern from the antenna, it is important that these effects be understood. The azimuth resolution and maximum probing depth of the radar depend on the antenna's beamwidth and the gain in the downward direction, respectively (Ulaby et al., 1982). Moreover, side lobes in the pattern may result in echoes from the side which are interpreted as coming from the main beam (Skolnik, 1980). When the true radiation characteristics within the ice sheet are known, the effects of the antenna on the radar performance can be predicted.

When calculating the antenna pattern within the ice sheet, the radiation into the surface must first be determined. Because their radiation characteristics into a dielectric half-space are well understood, dipole antennas have often been used with ice-probing radars (Clough, 1974). Unfortunately, dipoles are poorly suited for this application, because they have extremely wide beamwidths, with the maximum radiation being approximately 35 degrees from vertical (Annan, 1973). To improve the performance of the radar, a more complex system should be used. However, while the radiation from a simple dipole antenna into a dielectric half-space may be determined analytically, approximate methods must be used with more complex antenna systems.

Once the radiation into the surface is known, the effects of the ice density gradient on the pattern must be calculated. As the depth increases, the ice becomes more dense (Paterson, 1981) and its permittivity increases (Robin et al., 1969). Thus, energy propagating downward is refracted toward the normal, resulting in a reduction in beamwidth. Gudmansen (1971) derived a method to determine the paths energy rays will follow by treating the ice as a series of layers with a constant density. Clough (1974), on the other hand, used layers with densities which varied linearly with depth. Although both methods give accurate representations of the raypaths, no single closed-form equation can be used to represent the entire raypath since each uses discrete layers. As the energy is refrac-

Manuscript received by the Editor October 27, 1986; revised manuscript received April 30, 1987.
*Radar Systems and Remote Sensing Lab, University of Kansas, 2291 Irving Hill Drive, Lawrence, KS 66045-2969.

ted, it is focused into a smaller area resulting in an increase in the antenna gain. Robin et al. (1969) gave an equation for this increase based on the final path the ray will ultimately follow within the ice sheet. Although not explicitly stated, however, this equation is valid only for great depths and thus does not accurately give the gain increase at shallow depths.

Here we discuss a method to determine the radiation pattern at all depths within an ice sheet for a complex antenna structure placed directly on the ice surface. The radiation into the surface is determined using the well known method of moments (Harrington, 1968) for an antenna system over a homogeneous half-space. The raypaths of the energy are then determined by solving the geometric optics ray-tracing equation in closed form for a continuous exponential density gradient yielding the radiation pattern within the ice. The resulting pattern may be substituted directly into the radar equation with no further modification. A numerical example is then presented which demonstrates that the performance of an antenna system may be optimized for use with a probing radar using this technique. The antenna array analyzed is shown to perform better than a single dipole element used in the same capacity.

CALCULATION OF PATTERN WITHIN AN ICE SHEET

Radiation into the surface

The energy coupled into the surface of a dielectric half-space from an antenna placed directly on that surface may be calculated analytically for only a few simple configurations (Annan, 1973). However, when a more complex antenna is used, Maxwell's equations may be solved numerically by computer programs such as the Numerical Electromagnetic Code (NEC) (Breakall et al., 1985). NEC uses the method of moments, a popular method of solving integral equations, to determine the currents on individual segments of the antenna structure resulting from the antenna excitation (Harrington, 1968). To include the effects of interactions with the dielectric, the Sommerfeld integral is evaluated for elements near the dielectric surface. From the segment currents, the radiation pattern within the dielectric may be calculated easily.

NEC assumes a homogeneous half-space, but (as mentioned) the permittivity of the ice sheet increases with depth. Fortunately, most deep ice-probing radars use VHF or lower-frequency antennas whose far-field conditions are met before the ice permittivity has changed significantly. Thus, the fields within the top layer of the ice sheet may be determined from the far-field radiation over a homogeneous half-space whose permittivity is equal to that of the top layer of ice.

Raypaths within the ice sheet

Radiated energy in the far-field region of an antenna exhibits local plane-wave behavior (Stutzman et al., 1981). Thus, the propagation of energy within the ice sheet may be treated as rays with planar wavefronts beginning at the onset of the far-field region of the antenna. Furthermore, since the change in the ice permittivity from the surface to the onset of the far-field region is small, the refraction of plane waves between these two points is negligible. The rays may therefore be assumed to emanate from the ice surface with little inaccuracy.

Because of the plane-wave nature of the rays near the surface, geometric optics may be applied directly to these rays to determine their paths within the inhomogeneous ice sheet (Freehaufer, 1951). From this, an effective look angle and gain improvement for each ray may be calculated.

In polar ice (Evans, 1965), $\varepsilon' \gg \varepsilon''$, where ε' and ε'' are the real and imaginary components of the complex permittivity of the ice, respectively. Hence, the raypaths within the ice sheet will be determined solely by ε', and ε'' may be ignored in the ray-tracing calculations. However, it should be noted that ε'' will introduce significant propagation losses which must be considered when predicting the power received by a radar. Bogorodsky et al. (1985) have summarized the losses which can be expected.

The density of the ice is in general a function of depth only, so the ice sheet may be treated as a horizontally stratified medium. Thus, the radial distance traveled by a ray which begins at the surface is (Freehaufer, 1951)

$$r' = \int_0^z \frac{\zeta \, dz}{\sqrt{n^2(z) - \zeta^2}}, \tag{1}$$

where z is the depth within the ice, $n(z)$ is the refractive index of the ice, and

$$\zeta = n_0 \sin \gamma_0, \tag{2}$$

where n_0 is the refractive index at the surface and γ_0 is the angle of the ray with respect to the normal at the surface. Because the imaginary component of the complex permittivity of the ice is negligible, the refractive index is simply the square root of the real component of the relative permittivity.

Near the surface, the ice will have air bubbles trapped within it which yield a density less than that of pure ice (Paterson, 1981). As the depth increases, these bubbles are compressed into smaller volumes and the density increases. Finally, at great depths, the density approaches that of pure ice. The density may be accurately modeled by the relation (Robin et al., 1969)

$$\Delta = P - V \exp(Rz), \tag{3}$$

where Δ is the density of the ice, P is the maximum density of the ice (0.92 g/cm^3), and V and R are constants determined by a specific ice-sheet profile. Although this formula for the density is not exact, it holds within a couple of percent for both Antarctic and Greenland ice sheets. Note that since the density increases with depth, R is always negative.

Robin et al. (1969) introduced the empirical relation

$$n = 1.0 + 0.854\Delta, \tag{4}$$

which relates the refractive index of polar ice to its density. Jezek (1983) experimentally confirmed that equation (4) accurately predicts the velocity of propagation in a Greenland ice sheet and thus will also be valid for the calculations of the raypath.

By combining equations (3) and (4), a continuous representation of the refractive index of the ice sheet is obtained. Substituting the refractive index into equation (1) and evaluating the integral, the radial distance a ray has traveled when

it reaches a depth z is

$$r' = -\frac{\zeta}{R\sqrt{a}} \log \frac{V(2\sqrt{aX} + b\theta + 2a)}{\theta(2\sqrt{aX_v} + bV + 2a)}, \tag{5}$$

where

$$a = (1 + 0.854P)^2 - c^2,$$
$$b = -2(0.854)(0.854 + 1),$$
$$X = a + b\theta + d\theta^2,$$
$$X_v = a + bV + dV^2,$$
$$d = (0.854)^2,$$
$$\theta = V \exp(Rz),$$

and ζ was defined in equation (2). Because a continuous model of the refractive index was used, the radial position of any ray at any depth may be determined by a single evaluation of equation (5). Thus, it is not necessary to step the raypath through several discrete layers as in previous ray-tracing techniques (Clough, 1974; Gudmansen, 1971), which greatly reduces the calculation time required to determine a ray position.

Effective look angle

Figure 1 shows a typical raypath begining at the ice surface with an initial angle of γ_0. As the ray penetrates the ice sheet, it encounters an increasing refractive index and is focused toward the normal. The angle the ray makes with vertical at any depth may be calculated from Snell's law (Stratton, 1941):

$$\gamma' = \arcsin\left(\frac{n_0}{n} \sin \gamma_0\right). \tag{6}$$

Because the gradient in the refractive index is greatest near the surface due to the exponential nature of the density, the ray curvature is greatest near the surface. As the depth increases, the ray approaches a straight path whose angle is

$$\gamma'_{\min} = \arcsin\left(\frac{n_0}{n_{\max}} \sin \gamma_0\right), \tag{7}$$

where $n_{\max}$ is the maximum refractive index of ice = 1.79.

Because of the curvature of the ray, the actual angle between the source and a point, or the effective look angle of the ray, is different from the initial angle the ray must take to reach this point. This relation for the look angle is given by

$$\eta' = \arctan\left(\frac{r'}{z}\right), \tag{8}$$

where η' is the effective look angle of the ray.

As seen in Figure 1, the effective angle of the ray depends on the depth, even after the ray is following an essentially linear path. Moreover, it is always less than the initial angle. Thus, the beamwidth of an antenna radiating into an ice sheet is narrower than if it were radiating into a homogeneous medium. As the depth becomes very large, η' asymptotically approaches $\gamma'_{\min}$. The minimum effective angle for a ray therefore occurs as $z \to \infty$ and may be determined from equation (7).

Gain increase

As shown in Figure 2, a tube of adjacent rays extending from a point source over a homogeneous medium will enclose an area dA at a given distance from the source. When the same point source is located on an ice sheet whose density gradient is described by equation (3), the ray tube will be focused into a smaller area dA' at the same distance from the source and thus will exhibit a higher gain than it would have in a homogeneous ice sheet (Stutzman et al., 1982). Thus,

$$G_f = \frac{dA}{dA'}, \tag{9}$$

where G_f is the gain increase of a ray over its gain in a homogeneous medium. By allowing the spacing between the rays defining the ray tubes to approach zero, equation (9) will give the gain increase due to the refraction of an individual ray.

From Figure 2a,

$$dA = D^2 \sin \gamma_0 \, d\phi \, d\gamma_0. \tag{10}$$

Similarly, from Figure 2b,

$$dA' = r' \, d\phi \, dr' \cos \gamma' = r' \, d\phi \frac{dr'}{d\gamma_0} d\gamma_0 \cos \gamma'. \tag{11}$$

Substituting equations (10) and (11) into equation (9), the gain increase of a ray due to refraction is

$$G_f = \frac{D^2 \sin \gamma_0}{r' \dfrac{dr'}{d\gamma_0} \cos \gamma'}. \tag{12}$$

Equation (12) requires the derivative of r' with respect to γ_0 be evaluated. Using equation (1),

$$\frac{dr'}{d\gamma_0} = \frac{d}{d\gamma_0} \int_0^z \frac{\zeta \, dz}{\sqrt{n^2 - \zeta^2}}. \tag{13}$$

Reversing the order of differentiation and integration and solving,

$$\frac{dr'}{d\gamma_0} = r' \cot \gamma_0 + \frac{\zeta^2 n_0 \cos \gamma_0}{R} \times \left\{\frac{r'}{a\zeta} - \frac{2}{aq}\left[\frac{(b\theta - 2ad + b^2)}{\sqrt{X}} - \frac{(bV - 2ad + b^2)}{\sqrt{X_v}}\right]\right\}, \tag{14}$$

where a, b, d, X, and X_v are defined in equation (5) and $q = 4ad - b^2$. Since the parameters of equations (5) and (14) are identical, both may be evaluated simultaneously with little additional computation.

As was the case for the calculation of the ray position, the continuous nature of the modeled density gradient allows a closed-form relationship for the gain increase of a ray to be derived. The calculation time required using equations (14) is again much less than when the ice sheet is modeled by several discrete density layers.

The definition for the gain increase G_f of a ray given in equation (11) was chosen so that the distance D between the antenna and the area dA' may be used in the radar equation to represent the spreading loss within the ice sheet. From

Figure 2b, however, the ray tube appears to emanate from a point away from the antenna, whose distance to dA' is given by $D' \neq D$. Thus, the difference in spreading loss due to the difference between D and D' is included in G_f, and the gain increase of a ray continues to change well after it follows a linear path. As the depth gets very large, the difference between D and D' becomes negligible and the gain becomes constant. In this case,

$$dA' = D^2 \, d\phi \sin \gamma' \, d\gamma'. \tag{15}$$

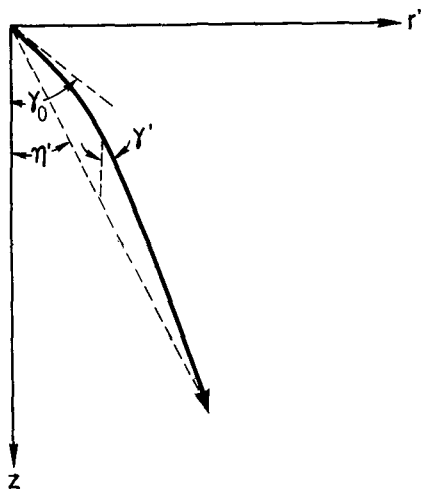

FIG. 1. Raypath within the ice sheet.

Hence, the gain increase of the ray as $z \to \infty$ is

$$G_f\Big|_{z\to\infty} = \frac{\sin \gamma_0 \, d\gamma_0}{\sin \gamma' \, d\gamma'}. \tag{16}$$

Using Snell's law, equation (16) may also be written as

$$G_f\Big|_{z\to\infty} = \frac{n_{\max}^2 \cos \gamma'}{n_0^2 \cos \gamma_0} = \frac{n_{\max}^2 \cos \gamma'}{n_0 \sqrt{n_0^2 - n_{\max}^2 \sin^2 \gamma'}}. \tag{17}$$

The right side of equation (17) is exactly the gain increase predicted by Robin et al. (1969) (valid only at great depths), which confirms that equation (9) accurately predicts the gain increase at great depths within the ice sheet.

Radiation pattern

The gain of the radiation pattern within the ice in the direction of the effective look angle η' of a ray is given by

$$G(\eta') = G_0 G_f, \tag{18}$$

where G_0 is the gain of the antenna radiation over a homogeneous medium with a permittivity equal to that of the top layer of ice in the direction of the initial angle (γ_0) of the ray. When all rays making up the surface energy coupling are considered, the gain at all look angles may be determined and the entire pattern within the ice may be constructed.

From equation (17), $G_f(\gamma_0)$ is greater for rays with large initial angles than for near-vertical rays. Thus, it is possible that side lobes may occur in the radiation pattern deep within the ice, although none were predicted by the radiation into a homogeneous dielectric (whether determined numerically by NEC or analytically for a simple antenna configuration). With

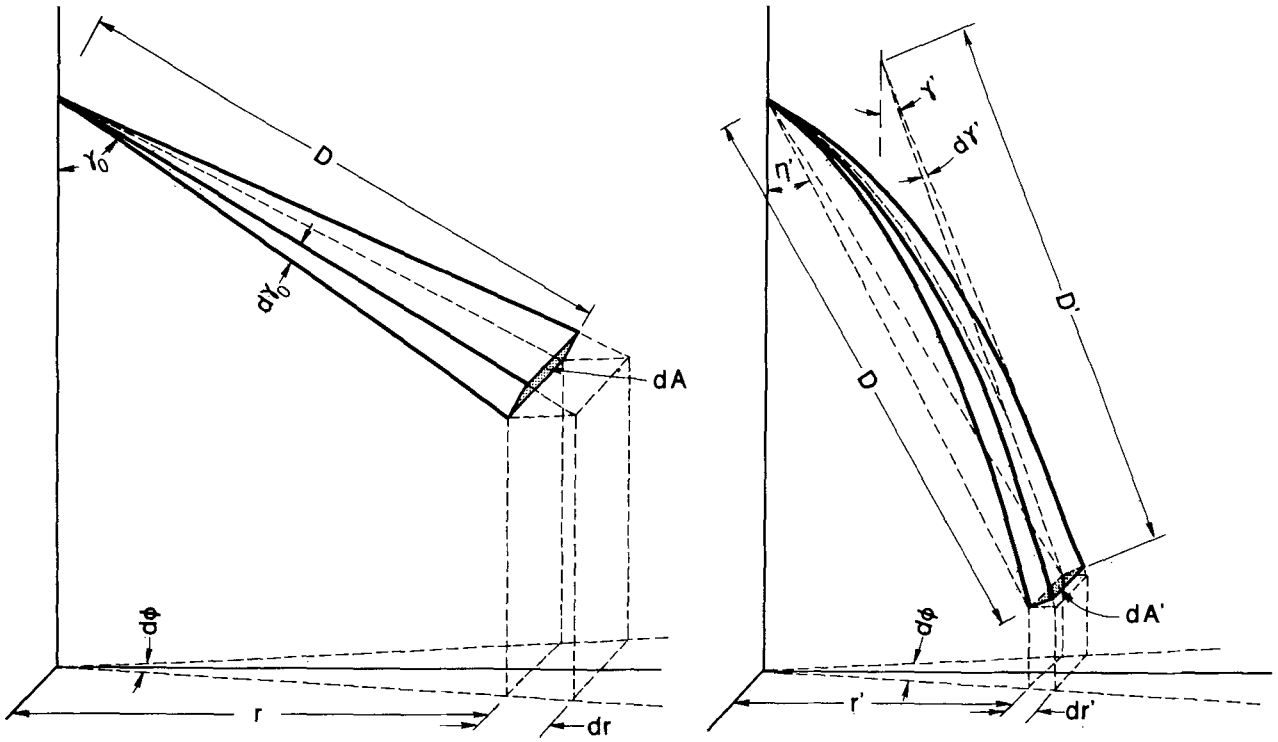

FIG. 2. Constant-energy ray tubes.

certain antenna configurations, the side lobes may actually have a greater gain than the radiation in the downward direction. Hence, when optimizing the antenna response, it is necessary to determine the radiation pattern at several depths within the ice sheet. If the final design is based solely on the predictions of energy coupling, certain undersirable effects of the refraction may go undetected.

Radiation pattern in the radar equation

The bedrock at the base of an ice sheet will have many point scatterers within the area illuminated by the antenna beam. The average power received by a radar from a target such as this is given by the area-extensive radar equation (Ulaby et al., 1982):

$$P_r = \frac{\lambda^2}{(4\pi)^3} \int_{\text{area illuminated}} \frac{P_t G^2 \sigma^0 \, dA}{D^4 L_p}, \tag{19}$$

where P_r is the power received, P_t is the power transmitted, G is the gain of the antenna as determined by equation (18), σ^0 is the average scattering cross-section per unit area of the target, D is the distance to the target, and L_p is the propagation loss. From the relation in equation (19), it is seen that any aspects of the performance of a radar which depend on the antenna pattern may be determined directly from the calculated pattern within the ice sheet. Note that if the scattering coefficient of the target varies with the angle of incidence, the actual angle the ray is following at the target γ should be used for determining the scattering cross-section, not the effective angle η'.

REPRESENTATIVE EXAMPLE

Antenna configuration

Figure 3 shows an antenna structure designed at the University of Kansas Radar Systems and Remote Sensing Lab specifically for use with an ice-probing radar whose center operating frequency is 150 MHz (West, 1986). 150 MHz was chosen as the operating frequency because it allowed a multielement array antenna of a manageable size, giving a significantly higher gain and narrower beamwidth than a single element, while avoiding excessive propagation losses due to the complex permittivity of the ice.

The performance of the antenna system was optimized by an iterative process. First, an initial configuration was constructed using the well known free-space antenna array theory. The true radiation pattern of the system within the ice when it was operating directly on the surface was then determined using the method described above. Once the true radiation was known, it was possible to predict modifications to the structure which would enhance its usefulness with a probing radar. The cycle was repeated until the best possible performance in terms of beamwidth, gain, side lobes, and bandwidth was reached.

The final antenna system consists of eight dipole elements, four driven elements (active) which are 3 inches above the ice surface, and four passive (parasitic) elements which are approximately one-quarter wavelength above the surface. The parasitic elements ensure that little energy is lost due to upward radiation. In the initial model, all the elements were one-half wavelength long and their centers were spaced by one-half wavelength, the optimum configuration for a free-space array operating at a single frequency. However, the analysis of the pattern within the ice showed that although this design had high downward gain and a tight beamwidth, unacceptably high side lobes were also present. It was found that by scaling the active elements down by a factor of 1.17 (the average of the refractive indices of air and the surface layer of ice), the side lobes could be eliminated while retaining good directivity and a narrow beamwidth. Furthermore, we determined that the radiation pattern would not vary significantly over the operating band of the radar (17 MHz) if the entire system was further scaled by a factor of 0.943. Thus, all elements in the array are shorter than one-half wavelength and the passive elements are somewhat longer than the active elements.

Curve fitting to the density gradient

Measured ice densities at different depths at Byrd Station in Antarctica (Clough, 1974) were fit to the form of equation (3) using a least-squares error criterion giving

$$V = 0.520 \text{ g/cm}^3, \tag{20a}$$

and

$$R = -0.033 \text{ m}^{-1}. \tag{20b}$$

Using this fit, the maximum error in the calculated refractive index, when compared to the refractive index determined from the measured ice densities, is less than 1.5 percent at depths greater than 2 m. At the surface, the error is 2.7 percent. Therefore, any errors in the calculated patterns introduced by the exponential density model will be small.

Radiation into the surface

The radiation into the surface of the ice sheet was determined using NEC to calculate the far-field radiation of the antenna located on a homogeneous half-space. The dielectric

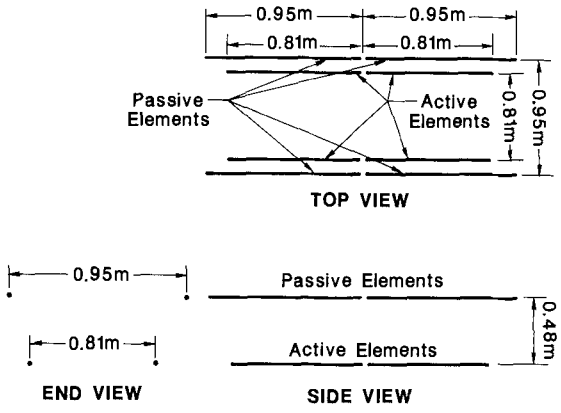

FIG. 3. Antenna system for use with an ice sheet-probing radar.

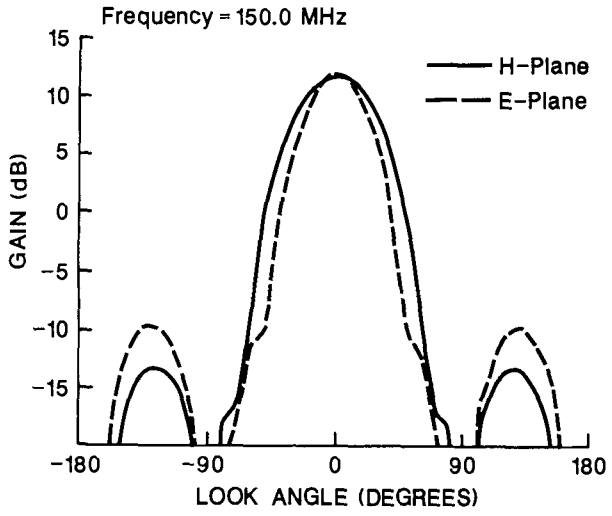

FIG. 4. Radiation into the surface of a homogeneous half-space, $\varepsilon_r = 1.8$.

constant of the half-space was set at 1.8, the value of the dielectric constant of the upper layer of ice. The results are shown in Figure 4. The pattern between look angles of −90 and 90 degrees represents the magnitude of the fields coupled into the ice, with 0 degrees representing straight down. All other look angles correspond to energy radiated into the air. As desired, the maximum radiation is at 0 degrees and very little energy is lost into the air.

The operating characteristics of the antenna system can only be affected by the dielectric material within its near field. The distance to the beginning of the far field of an antenna is given by (Balanis, 1982)

$$D_{ff} = \frac{2d^2}{\lambda}, \tag{21}$$

where d is the maximum dimension of the antenna and λ is the operating wavelength. Within the ice, D_{ff} is approximately 4 m for the system being analyzed. At this depth, the dielectric constant of the ice has increased to 1.9. A change of this magnitude will have little effect on the radiated fields at the onset of the far-field region.

Effective look angles and gain improvements

From the Appendix, the geometric optics approximation of the energy raypaths is accurate when

Table 1. Effective angle of rays for any antenna within the Byrd station ice sheet.

		Depth of observation point (m)							
		50	100	150	200	300	400	600	1000
Initial angle of ray (degrees)	0	0.00	0.00	0.00	0.00	0.00	0.00	0.00	0.00
	10	8.60	8.14	7.93	7.81	7.69	7.63	7.58	7.53
	20	17.15	16.20	15.77	15.53	15.30	15.17	15.05	14.96
	30	25.56	24.10	23.43	23.07	22.70	22.51	22.32	22.17
	40	33.75	31.73	30.80	30.30	29.78	29.51	29.25	29.04
	50	41.59	38.94	37.72	37.06	36.36	36.01	35.65	35.36
	60	48.90	45.55	44.00	43.13	42.23	41.77	41.30	40.92
	70	55.45	51.31	49.36	48.27	47.11	46.51	45.89	45.39
	80	60.94	55.94	53.54	52.17	50.68	49.90	49.10	48.43

Table 2. Gain increases of rays for any antenna within the Byrd station ice sheet.

		Depth of observation point (m)							
		50	100	150	200	300	400	600	1000
Initial angle of ray (degrees)	0	1.29	1.78	2.00	2.13	2.26	2.33	2.39	2.45
	10	1.30	1.79	2.02	2.15	2.28	2.35	2.42	2.47
	20	1.32	1.83	2.08	2.21	2.35	2.43	2.50	2.56
	30	1.36	1.91	2.18	2.33	2.49	2.57	2.66	2.72
	40	1.43	2.03	2.34	2.52	2.71	2.81	2.91	2.99
	50	1.54	2.24	2.61	2.82	3.06	3.19	3.32	3.42
	60	1.71	2.56	3.03	3.31	3.63	3.80	3.98	4.13
	70	2.02	3.10	3.72	4.12	4.57	4.83	5.10	5.33
	80	2.54	3.99	4.90	5.50	6.25	6.69	7.19	7.64

$$f \gg \frac{0.854c}{2\pi n_0^2} |VR|, \tag{22}$$

where f is the frequency of operation and V and R are constants determined by a specific density profile of the ice sheet. Using the values determined in equation (20), f becomes

$$f \gg 0.372 \text{ Hz}. \tag{23}$$

Since the antenna being modeled has an operational frequency of 150 MHz, the calculated raypaths and gain increases will be accurate.

Tables 1 and 2 give the effective look angles and gain increases, respectively, of rays with several different initial look angles at various depths within the ice sheet. As expected, rays which begin with large look angles are refracted more than near-vertical rays; hence, their effective angles deviate more from their initial angles. Also, the focusing effect at large angles is more pronounced, so the gain increases for these rays are greater. Since the density of the ice is effectively constant at depths below 150 m, the rays follow linear paths in this region. However, the effective look angles and gain increases still vary at depths far greater than 150 m, as predicted. As the depth gets very large, they approach the limits given by equations (7) and (16).

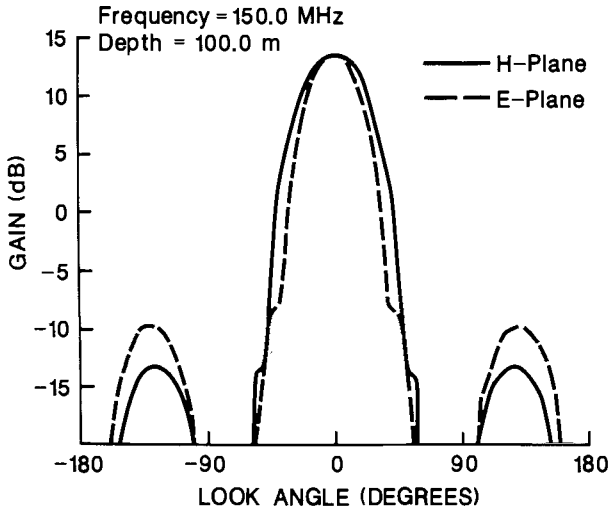

FIG. 5a. Radiation pattern 100 m within the Byrd station ice sheet.

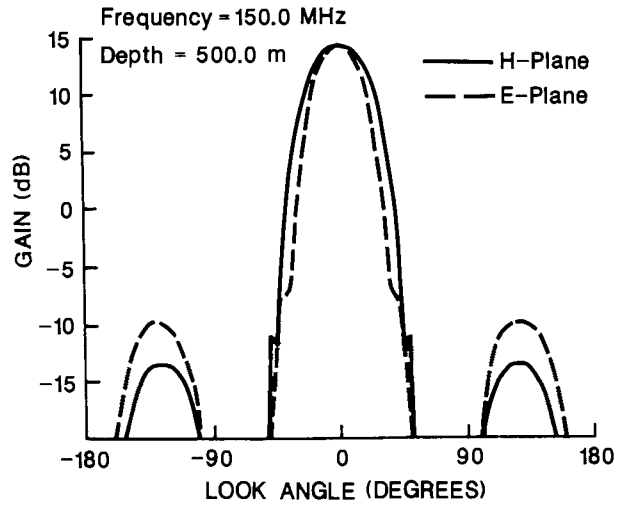

FIG. 5b. Radiation pattern 500 m within the Byrd station ice sheet.

Patterns within the ice sheet

The results in Tables 1 and 2 were applied to the radiation into the surface to give radiation patterns at depths of 100 m and 500 m within the ice sheet, shown in Figures 5a and 5b, respectively. At a depth of 100 m, the beamwidths in both the electric-field plane (E plane, parallel to the dipole elements) and the magnetic-field plane (H plane, perpendicular to the dipole elements) have become significantly narrower than at the surface and the gain has improved. These effects are more pronounced at 500 m depth, but Tables 1 and 2 show there will be little additional improvement below 500 m.

The calculated patterns show the antenna is well suited for use with an ice-probing radar and represents a significant improvement over a single-dipole element. The maximum gain is in the downward direction at all depths, as desired; the gain is greater than 12 dB at the surface and approaches 15 dB at depths greater than 500 m. The 3 dB beamwidths at the surface are approximately 50 degrees in the H plane and 40 degrees in the E plane. As the depth increases, these beamwidths reduce to approximately 35 degrees and 30 degrees, respectively. There are no significant side lobes at any depth. A radar using this antenna will have a much finer azimuth resolution and a greater depth of penetration than when using a dipole radiator.

CONCLUSIONS

A technique to determine the radiation pattern of a complex antenna system placed directly on the surface of an ice sheet at any depth within the ice has been demonstrated. The radiation into the surface is determined by applying the method of moments to the antenna system placed over a homogeneous dielectric half-space whose relative permittivity is equal to that of the surface ice. The effective look angles and gain increases of rays resulting from the density gradient of the ice are determined using geometric optics. Since the ray-tracing equation is solved in closed form for a typical density profile, calculation of these effects is much simpler than using previous techniques.

A numerical example illustrates this technique. The radiation patterns of an antenna system designed specifically for a probing radar have been calculated at two different depths within an ice sheet. These calculations show that the maximum radiation is in the downward direction at all depths, as desired, and no significant side lobes appear due to the greater gain increase of rays away from vertical. The 3 dB beamwidths are narrower than they would have been had the ice sheet been homogeneous, and the gain in the downward direction improves as the depth is increased. The overall radiation performance of the antenna analyzed has been shown to be well suited for use with an ice-probing radar.

Use of this technique gives several benefits to those involved

in the design or use of ice-probing radars. Since the radiation pattern of virtually any system can now be determined in the environment in which it will actually be used, the design procedure of a suitable antenna is greatly simplified. The effects of any changes in the antenna configuration can be quickly determined, so the system response can be optimized for use with a probing radar through an iterative process. Moreover, the data received can be more easily interpreted when the radiation pattern is known. The effects of the antenna on the received signals can be calculated and included in the data analysis. Characteristics such as the spacing between two received targets or the strength of a reflection from a target can be more readily determined. Hence, this technique provides for a more accurate profile of the structure of the ice sheet.

ACKNOWLEDGMENT

This work was supported by funding through the National Science Foundation grant DPP-8300450.

REFERENCES

Annan, A. P., 1973, Radio interferometry depth sounding, Part 1—theoretical discussion: Geophysics, **38**, 557–580.
Balanis, C., 1982, Antenna theory: McGraw-Hill Book Co.
Bogorodsky, V. V., Bentley, C. R., and Gudmansen, P., 1985, Radioglaciology: Klewer.
Breakall, J. K., Burke, G. J., and Miller, E. K., 1985, The Numerical Electromagnetics Code (NEC): 6th Sympos. and Tech. Exhibition on Electromagnetic Compatibility, Zurich.
Clough, J. W., 1974, Radio wave propagation in the Antarctic ice sheet: Ph.D. thesis, Univ. of Wisconsin.
Evans, S., 1963, Radio techniques for the measurement of ice thickness: Polar Record, **11**, 406–410.
——— 1965, Electric properties of ice and snow—a review: J. Glaciology, **5**, 773–792.
Freehaufer, J. E., 1951, Geometric optics, *in* Kerr, D. E., Ed., Propagation of short radio waves: McGraw-Hill Book Co.
Gudmansen, P., 1971, Electromagnetic probing of ice, *in* Wait, J. R., Ed., Electromagnetic probing in geophysics: Golem.
Harrington, R. F., 1968, Field computation by moment method: Krieger.
Harrison, C. H., 1973, Radio echo sounding of horizontal layers in ice: J. Glaciology, **66**, 383–397.
Jezek, K. C., 1983, Measurements of radar wave speeds in polar glaciers using a down-hole radar target technique: Cold Regions Sci. Tech., **8**, 199–208.
Paterson, W. S. B., 1981, The physics of glaciers: Pergamon Press.
Robin, G. deQ., Evans, S., and Bailey, J. T., 1969, Interpretations of radio echo sounding in polar ice sheets: Phil. Trans., Roy. Soc. of London, **A-265**, 437–505.
Skolnik, M. I., 1980, Introduction to radar systems: McGraw-Hill Book Co.
Stratton, J. A., 1941, Electromagnetic theory: McGraw-Hill Book Co.
Stutzman, W. L., and Theil, G. A., 1981, Antenna theory and design: Wiley and Sons.
Ulaby, F. T., Moore, R. K., and Fung, A. K., 1982, Microwave remote sensing: active and passive: Addison-Wesley Publ. Co.
West, J. C., 1986, Design and analysis of an antenna system for use with a coherent ice probing radar: M.S. thesis, Univ. of Kansas.

APPENDIX

LIMITATIONS TO RAY TRACING

The ray-tracing equation as given in equation (1) is accurate only when a high-frequency approximation can be made. The validity of this approximation may be checked by the inequality (Freehaufer, 1951)

$$\frac{|\nabla n|}{kn^2} \ll 1, \tag{A-1}$$

where ∇n is the gradient of n and k is the wavenumber in free space. Using the ice-sheet profile model given by equations (3) and (4), equation (A-1) need only be evaluated at the surface where the density gradient, and hence the refractive index gradient, are maximum. Since the refractive index is a function of depth only,

$$\nabla n_{\max} = \left.\frac{dn}{dz}\right|_{z=0}. \tag{A-2}$$

Substituting equation (4) into equation (A-2) and knowing $k = 2\pi f/c$, where f is the frequency and c is the speed of light in free space, the inequality may be reduced to

$$f \gg \frac{0.854c}{2\pi n^2}\,|VR|, \tag{A-3}$$

where V and R are constants determined by a specific density profile.